Graph Optimization Approach to Range-Based Localization

Xu Fang, Chen Wang, Thien-Minh Nguyen, and Lihua Xie, *Fellow, IEEE*

***Abstract*—In this article, we propose a general graph optimization-based framework for localization, which can accommodate different types of measurements with varying measurement time intervals. Special emphasis will be on range-based localization. Range and trajectory smoothness constraints are constructed in a position graph, then the robot trajectory over a sliding window is estimated by a graph-based optimization algorithm. Moreover, convergence analysis of the algorithm is provided, and the effects of the number of iterations and window size in the optimization on the localization accuracy are analyzed. Extensive experiments on quadcopter under a variety of scenarios verify the effectiveness of the proposed algorithm and demonstrate a much higher localization accuracy than the existing range-based localization methods, especially in the altitude direction.**

***Index Terms*—Graph optimization approach, range-based localization, two-dimensional (2-D) and three-dimensional (3-D) spaces, ultrawide band radio.**

I. Introduction

ACCURATE, efficient and reliable localization plays important roles in real-time robot-related applications [1]–[6], such as formation, swarming, and target search. The vision-based simultaneous localization and mapping (SLAM) technologies [7] have an unacceptable drift over a long run without odometer correction and need significant computational resources for dense mapping, which is not suitable for ultralow power processors. The WiFi-based localization [8] has the problem of estimation fluctuations caused by the variation of signals and its low localization accuracy makes it inapplicable to robots such as unmanned aerial vehicles (UAVs). Optical motion capture systems can provide millimeter level of localization accuracy [9], but they are very expensive and confined to limited space.

Manuscript received April 18, 2019; revised November 10, 2019; accepted December 27, 2019. This work was supported in part by ST Engineering-NTU Corporate Laboratory under the NRF Corporate Lab, University Scheme and National Natural Science Foundation of China under Grant 61720106011. This article was recommended by Associate Editor C. J. F. Silvestre. *(Corresponding author: Lihua Xie.)*

Xu Fang, Thien-Minh Nguyen, and Lihua Xie are with the School of Electrical and Electronic Engineering, Nanyang Technological University, Singapore 639798 (e-mail: fa0001xu@e.ntu.edu.sg; e150040@e.ntu.edu.sg; elhxie@ntu.edu.sg).

Chen Wang was with the School of Electrical and Electronic Engineering, Nanyang Technological University, Singapore 639798. He is now with Robotics Institute, Carnegie Mellon University, Pittsburgh, PA 15213 USA (e-mail: chenwang@dr.com).

Color versions of one or more of the figures in this article are available online at http://ieeexplore.ieee.org.

Digital Object Identifier 10.1109/TSMC.2020.2964713

An alternative method which utilizes the ultrawideband (UWB) technology [10] has attracted researchers' attention due to its robustness to multipath and nonline of sight (NLOS) effects. The UWB modules with known positions are referred to anchors. Robots carrying UWB modules are able to exchange information and calculate their distances to anchors by measuring the time of flight of signal, which are then used for estimating their own positions.

However, there are limitations of existing range-based localization algorithms. First, many algorithms [11]–[13], such as multilateration and multidimensional scaling (MDS) algorithms leveraging on optimization require that the mobile robot receive multiple concurrent range measurements. They may have relatively low localization accuracy when the range sensors cannot support multichannels. For example, the UWB sensors usually use a single wireless channel. The neglect of minor time difference between consecutive measurements brings localization error for the mobile robot.

Second, some algorithms consider such minor time difference, but need an accurate kinematic model. The representative examples are moving horizon estimation (MHE) [14] and the filter-based methods such as extended Kalman filter (EKF) [15]–[18]. However, an accurate kinematic model may be hard to obtain due to the complex structure of robots, and a simplified or linearized kinematic model degrades their localization performance. Last, the recent trend toward machine learning-based methods stimulates a new wave of research, but generally it is still difficult to achieve good performance in real-time [19]–[21]. These challenges open space for accurate, reliable, and robust localization techniques.

From the experimental results in the existing range-based localization methods [11], [17], [22], [23], we find that their performance in the altitude direction is generally not as good as other directions. Some possible solutions include: 1) adding altitude sensors, such as laser beam or lidar to measure the altitude, but it requires the ground to be even and 2) placing anchors on the ceiling, but it may also be difficult for many environments.

The graph optimization approach was originated from the vision-based SLAM technology [7], [24]. By using this technique, we shall present a general graph optimization-based framework for localization, which can accommodate different kinds of measurements with varying measurement time intervals. Special emphasis will be on range-based localization, which mitigates the requirements of an accurate kinematic model, multichannel support and high power processors, and improves the localization performance. It is worth noting that

the existing geometry optimization methods [25]–[27] are suitable for estimating a static sensor network, which may not applicable for localizing a mobile robot.

The proposed range-based localization jointly imposes the range and trajectory smoothness constraints over a sliding trajectory window that has several characteristics.

1) It removes the dependence on the kinematic model and the requirement of receiving concurrent multiple range measurements.
2) It estimates the trajectory over a window instead of single position estimation, and can be implemented real-time in some low power systems.
3) It is robust to outliers due to fusion with an outlier rejection algorithm.
4) From the experimental results, it is observed that the localization accuracy is much improved, especially in the altitude direction. This article is based on our previous works [28], [29].

The main contributions of this article are summarized as follows.

1) A general localization framework based on a graph optimization approach is proposed, which can accommodate different kinds of measurements with varying measurement time intervals. Special emphasis will be on range-only-based localization and range-orientation-based localization
2) Stability analysis of the algorithm is provided, and the effects of the number of iterations and window size in the optimization on the localization accuracy are analyzed.
3) The experimental results https://youtu.be/UuMBSrCEs 6Q on quadcopter demonstrate its stability as well as much higher localization accuracy than existing range-based algorithms, especially in the altitude direction without the need of placing anchors on the ceiling or adding altitude sensors.

This article is organized as follows. Section II proposes a general framework for localization. The basic concepts, problem description, problem formulation and special emphases on range-only-based localization and range-orientation-based localization are presented, respectively. In Section III, the optimization algorithm and computational complexity analysis are provided. Section IV presents the stability analysis. Section V provides the details of experimental results. Section VI ends this article with conclusions.

II. General Framework for Localization

A. Basic Concepts and Problem Description

Considering the robot motion in three-dimensional (3-D) space, its pose can be represented by a transformation matrix $\mathbf{P}$

$$\mathbf{P} = \begin{bmatrix} \mathbf{R} & \mathbf{t} \\ \mathbf{0} & 1 \end{bmatrix}, \quad \mathbf{R} \in \mathbb{R}^{3\times 3}, \quad \mathbf{t} \in \mathbb{R}^3 \tag{1}$$

where $\mathbf{R}$ is the rotation matrix, and $\mathbf{t}$ is the translation vector. The rotation matrix $\mathbf{R}$ and transformation matrix $\mathbf{P}$ belong to the lie groups SO(3) and SE(3) [30], respectively. The rotation matrix $\mathbf{R}$ and transformation matrix $\mathbf{P}$ can be represented by vectors ω and ϵ via an exponential mapping, i.e.,

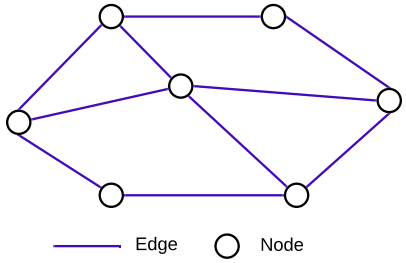

Fig. 1. General framework for localization.

$$\begin{aligned} &\epsilon = (\omega, \mathbf{u})^T \in \mathbb{R}^6, \omega = (\omega_1, \omega_2, \omega_3)^T \in \mathbb{R}^3, \mathbf{u}^T \in \mathbb{R}^3 \\ &\omega_\times = \begin{bmatrix} 0 & -\omega_3 & \omega_2 \\ \omega_3 & 0 & -\omega_1 \\ -\omega_2 & \omega_1 & 0 \end{bmatrix}, \quad \epsilon_\times = \begin{bmatrix} \omega_\times & \mathbf{u}^T \\ \mathbf{0} & 0 \end{bmatrix} \\ &\mathbf{R} = \exp(\omega_\times), \quad \mathbf{P} = \exp(\epsilon_\times). \end{aligned} \tag{2}$$

The rotation matrix $\mathbf{R}$ and transformation matrix $\mathbf{P}$ span over non-Euclidean spaces. Based on (2), the functions $\mathbf{log}_{\mathrm{SO(3)}}(\cdot)$ and $\mathbf{log}_{\mathrm{SE(3)}}(\cdot)$ are defined such that the rotation matrix $\mathbf{R}$ and transformation matrix $\mathbf{P}$ in non-Euclidean spaces are mapped into their corresponding Euclidean spaces

$$\mathbf{log}_{\mathrm{SO(3)}}(\mathbf{R}) = \omega, \quad \mathbf{log}_{\mathrm{SE(3)}}(\mathbf{P}) = \epsilon. \tag{3}$$

Then, the conventional optimization methods, such as Levenberg–Marquardt method applicable to a Euclidean space can be used for rotation estimation and transformation estimation.

The graph $G = \{\mathcal{V}, \mathcal{E}\}$ consisting of nodes and edges in Fig. 1 shows the structure of the proposed localization, where $\mathcal{V} = \{v_1, v_2, \ldots, v_n\}$ is the node set, and $\mathcal{E} \subseteq \mathcal{V} \times \mathcal{V}$ is the edge set. Denoted by $(v_i, v_j) \subseteq \mathcal{E}$ an edge of G. Each edge represents a constraint between two nodes. The graph G allows the fusion of different measurements by imposing constraints on the nodes. The problem is how to localize the nodes based on the constraints. For example, if each node in the graph G represents a mobile robot, some robots are equipped with a global positioning system (GPS) and know their own positions, while the rest do not know their own positions. The problem becomes how to localize the rest robots based on the known positions of some robots and the constraints among the robots.

Each edge (v_i, v_j) connects two nodes v_i, v_j, and the translations, rotations, and transformations of the two nodes v_i, v_j are denoted by $\mathbf{t}_i, \mathbf{t}_j \in \mathbb{R}^3$, $\mathbf{R}_i, \mathbf{R}_j \in \mathbb{R}^{3\times 3}$, and $\mathbf{P}_i, \mathbf{P}_j \in \mathbb{P}^{4\times 4}$, respectively. There are four kinds of constraints.

1) Range Constraint: Denoted by $d_{ij} \in \mathbb{R}$ the range measurement between nodes v_i, v_j. The range constrained equation is defined as

$$E_r(\mathbf{t}_i, \mathbf{t}_j) = w_r^{ij} \cdot \rho(e_r^{ij}) \tag{4a}$$

$$e_r^{ij} = d_{ij} - \|\mathbf{t}_i - \mathbf{t}_j\|_2 \tag{4b}$$

where $w_r^{ij} \in \mathbb{R}$ is the weight. $\|\cdot\|_2$ is the Euclidean norm of a vector or the spectral norm of a matrix. $\rho(\cdot)$ is the Pseudo-Huber loss function defined as $\rho(\varrho) = \xi^2(\sqrt{1 + (\varrho/\xi)^2} - 1)$ where $\xi > 0$ is the slope parameter.

2) Relative Translation Constraint: Denoted by $\mathbf{l}_{ij} \in \mathbb{R}^3$ the relative translation measurement between nodes v_i, v_j. The relative translation constrained equation is designed as

$$E_t(\mathbf{t}_i, \mathbf{t}_j) = \rho\left(\sqrt{\mathbf{e}_t^{ij^T} \mathbf{w}_t^{ij} \mathbf{e}_t^{ij}}\right) \tag{5a}$$

$$\mathbf{e}_t^{ij} = \mathbf{l}_{ij} - (\mathbf{t}_i - \mathbf{t}_j) \tag{5b}$$

where $\mathbf{w}_t^{ij} \in \mathbb{R}^{3\times3}$ is the weight.

3) Relative Rotation Constraint: Denoted by $\mathbf{u}_{ij} \in \mathbb{R}^{3\times3}$ the relative rotation measurement between nodes v_i, v_j. The relative rotation constrained equation is designed as

$$E_o(\mathbf{R}_i, \mathbf{R}_j) = \rho\left(\sqrt{\mathbf{e}_o^{ij^T} \mathbf{w}_o^{ij} \mathbf{e}_o^{ij}}\right) \tag{6a}$$

$$\mathbf{e}_o^{ij} = \mathbf{log}_{\mathrm{SO(3)}}\left(\mathbf{u_{ij}} \cdot (\mathbf{R_i R_j})^{-1}\right) \tag{6b}$$

where $\mathbf{w}_o^{ij} \in \mathbb{R}^{3\times3}$ is the weight, and function $\mathbf{log}_{\mathrm{SO(3)}}(\cdot)$ is defined in (3).

4) Relative Transformation Constraint: Denoted by $\mathbf{q}_{ij} \in \mathbb{R}^{4\times4}$ the relative transformation measurement between nodes v_i, v_j. The relative transformation constrained equation is designed as

$$E_p(\mathbf{P}_i, \mathbf{P}_j) = \rho\left(\sqrt{\mathbf{e}_p^{ij^T} \mathbf{w}_p^{ij} \mathbf{e}_p^{ij}}\right) \tag{7a}$$

$$\mathbf{e}_p^{ij} = \mathbf{log}_{\mathrm{SE(3)}}\left(\mathbf{q}_{ij} \cdot (\mathbf{P}_i \mathbf{P}_j)^{-1}\right) \tag{7b}$$

where $\mathbf{w}_p^{ij} \in \mathbb{R}^{6\times6}$ is the weight, and function $\mathbf{log}_{\mathrm{SE(3)}}(\cdot)$ is defined in (3).

B. Problem Formulation

For the node set $\mathcal{V} = \{v_1, v_2, \ldots, v_n\}$, the translations $\mathbf{t} = (\mathbf{t}_1^T, \mathbf{t}_2^T, \ldots, \mathbf{t}_n^T)^T$ and transformations $\mathbf{P} = (\mathbf{P}_1^T, \mathbf{P}_2^T, \ldots, \mathbf{P}_n^T)^T$ of the nodes can be estimated, respectively, by solving the following cost functions (8) and (9)

$$F(\mathbf{t}) = \sum_{(v_i, v_j) \subseteq \mathcal{E}} \left(E_r^{ij} + E_t^{ij}\right) \tag{8a}$$

$$\hat{\mathbf{t}} = \arg\min F(\mathbf{t}) \tag{8b}$$

where $\hat{\mathbf{t}} = (\hat{\mathbf{t}}_1^T, \hat{\mathbf{t}}_2^T, \ldots, \hat{\mathbf{t}}_n^T)^T$ are the estimated translations

$$F(\mathbf{P}) = \sum_{(v_i, v_j) \subseteq \mathcal{E}} \left(E_r^{ij} + E_t^{ij} + E_o^{ij} + E_p^{ij}\right) \tag{9a}$$

$$\hat{\mathbf{P}} = \arg\min F(\mathbf{P}) \tag{9b}$$

where $\hat{\mathbf{P}} = (\hat{\mathbf{P}}_1^T, \hat{\mathbf{P}}_2^T, \ldots, \hat{\mathbf{P}}_n^T)^T$ are estimated transformations.

Remark 1: For this general framework, we provide a corresponding application platform https://github.com/wang-chen/localization, which can accommodate different kinds of measurements for localization. The proposed general framework is inspired by the vision-based SLAM technology [7], [24]. In the SLAM technology, vision measurement is indispensable, but in our framework, the mobile robot can be localized without vision measurement.

Remark 2: The weights w_r^{ij}, $\mathbf{w}_t^{ij}$, $\mathbf{w}_o^{ij}$, and $\mathbf{w}_p^{ij}$ in (4)–(7) can be chosen based on their measurement accuracy. Denote the covariance of a measurement noise by σ^2. The most straightforward way is to set $\mathbf{w} = [1/(\sigma^2 + 1)]$. Note that the 1 in the denominator helps prevent singularity when σ^2 is very small.

TABLE I
COMPARISON WITH EXISTING EKF-BASED OR MHE-BASED RANGE LOCALIZATION METHODS

Methods	Measurements	Localization
EKF [16]	Range, Acceleration, Angular rate	2-D,3-D
EKF [31]	Range, Orientation, Odometry	2-D
EKF [17]	Range, Acceleration	2-D
MHE [32]	Range, Translation Speed, Rotational Speed	2-D
MHE [33]	Range, Velocity, Odometry	2-D
MHE [34]	Range, Translation Speed, Rotational Speed	2-D
MHE [35]	Range, Orientation, Altitude	3-D
MHE [36]	Range, Acceleration, Angular rate, GNSS	3-D
Our method	Range	2-D,3-D

GNSS: Global navigation satellite system
Our method: The proposed range-only based localization

Based on the proposed general framework, in this article, special emphasis will be on range-only-based localization and range-orientation-based localization. The structure of the range-based localization consisting of several fixed anchors and a mobile robot is shown in Fig. 2. For this special structure, the constraints can be divided into two categories.

1) *Range Constraint:* The constraint between the robot and an anchor.
2) *Trajectory Smoothness Constraint:* The constraint between adjacent robot translations.

C. Range-Only-Based Localization

In this part, we focus on a range-only-based localization. Compared with the EKF-based or MHE-based range localization algorithms [16], [17], [31]–[36] which use several kinds of measurements for localization shown in Table I, the proposed method only needs range measurements.

1) Range Constrained Equation: The robot translation at time instant k is denoted by $\mathbf{t}_k \in \mathbb{R}^3$, so that the robot trajectory can be denoted as $\mathbf{t} = (\mathbf{t}_1^T, \mathbf{t}_2^T, \ldots, \mathbf{t}_k^T)^T$. Our UWB ranging algorithm uses two-way time of flight measurement to calculate the range. A mobile robot equipped with a UWB module at translation $\mathbf{t}_k$ is able to range to one of the fixed UWB anchors at translation $\mathbf{t}_a^k$ shown in Fig. 2. The corresponding range measurement between $\mathbf{t}_k$ and $\mathbf{t}_a^k$ is denoted by d_k, which is obtained by the multiplication of light speed c and the measurement of time of flight

$$d_k = c\frac{Q_{ks} - Q_{kr}}{2} + \eta_k = \left\|\mathbf{t}_k - \mathbf{t}_a^k\right\|_2 + \eta_k \tag{10}$$

where Q_{ks} and Q_{kr} are the synchronized time instants when the UWB ranging radio is sent and received relative to the robot's clock, respectively. η_k is the bounded range measurement noise with $|\eta_k| \leq \eta$. By applying the 3-σ rule under the assumption that the range measurement noise η_k in (10) follows an approximately normal distribution, we get $\eta_k \sim \mathbb{N}(0, \sigma_r^2)$ with variance $\sigma_r^2 = (\eta^2/9)$. At time instant k, the range constrained equation E_r^k is defined as

$$E_r^k = w_r^k \cdot \rho(e_r^k) \tag{11a}$$

$$e_r^k = d_k - \left\|\mathbf{t}_k - \mathbf{t}_a^k\right\|_2 \tag{11b}$$

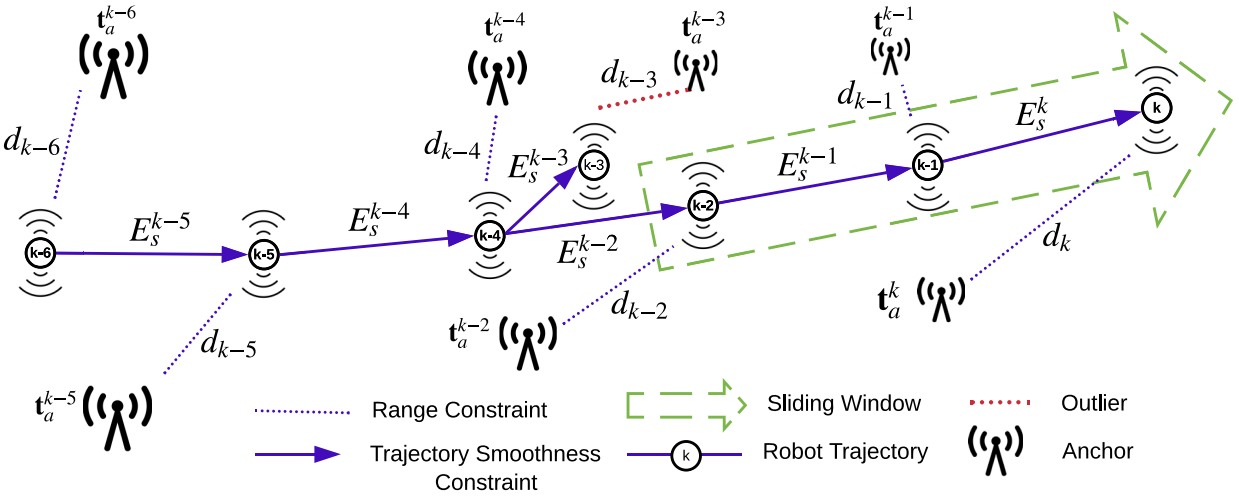

Fig. 2. Proposed range-based localization framework is shown in this figure. Each edge represents a constrained equation. At each time instant k, we construct a range constrained equation E_r^k and a trajectory smoothness constrained equation E_s^k. If the robot received a measurement outlier, the corresponding range constrained equation, such as E_r^{k-3} and trajectory smoothness constrained equation, such as E_s^{k-3} will not be added to the cost function.

where w_r^k is the weight given by

$$w_r^k = \frac{\iota^2}{\sigma_r^2 + \iota^2} \tag{12}$$

where ι is a free-parameter.

Remark 3: From Remark 2, the weight can be set as $w_r^k = [1/(\sigma_r^2 + 1)]$. To be more flexible, we add another free parameter ι to shrink σ_r. Then we have $w_r^k = [1/(\sigma_r^2/\iota^2 + 1)] = [\iota^2/(\sigma_r^2 + \iota^2)]$, where the square is to make it positive.

2) Trajectory Smoothness Constrained Equation: Equation (11) only gives constraints on a set of sparse points and fails to form a smooth trajectory. To solve this problem, a trajectory smoothness constrained equation between adjacent robot translations is needed. The moving equation between adjacent translations $\mathbf{t}_k$ and $\mathbf{t}_{k-1}$ is

$$\mathbf{t}_k = \mathbf{t}_{k-1} + \mathbf{r}_k \tag{13}$$

where $\mathbf{r}_k$ is the relative translation between translations $\mathbf{t}_k$ and $\mathbf{t}_{k-1}$. One issue is that the relative translation $\mathbf{r}_k$ is unknown, but we have

$$\|\mathbf{r}_k\|_2 = \|\mathbf{t}_k - \mathbf{t}_{k-1}\|_2 \leq v_{\max} \cdot \Delta T_k \tag{14}$$

where $v_{\max}$ is the maximum velocity of the robot. ΔT_k is the time interval between translations $\mathbf{t}_k$ and $\mathbf{t}_{k-1}$. Similarly, by applying the 3-σ rule under the assumption that the relative distance $\|\mathbf{r}_k\|_2$ follows an approximately normal distribution, we get $\|\mathbf{r}_k\|_2 \sim \mathbb{N}(0, (\sigma_s^k)^2)$ with variance $(\sigma_s^k)^2 = [(v_{\max} \cdot \Delta T_k)^2/9]$. Then, a trajectory smoothness constrained equation E_s^k between adjacent translations $\mathbf{t}_k$ and $\mathbf{t}_{k-1}$ is defined as

$$E_s^k = w_s^k \cdot \rho\left(e_s^k\right) \tag{15a}$$

$$e_s^k = \|\mathbf{t}_k - \mathbf{t}_{k-1}\|_2 \tag{15b}$$

where w_s^k is the weight designed as

$$w_s^k = \frac{\iota^2}{\left(\sigma_s^k\right)^2 + \iota^2} \tag{16}$$

where ι is a free-parameter.

3) Cost Function: At any time instant k when a range measurement d_k is received, we construct a range constrained equation E_r^k (11) and a trajectory smoothness constrained equation E_s^k (15), thus a trajectory $\mathbf{t} = (\mathbf{t}_1^T, \mathbf{t}_2^T, \ldots, \mathbf{t}_k^T)^T$ can be estimated by solving the following cost function:

$$F(\mathbf{t}) = \sum_{i=1}^{k} \left(E_r^i + E_s^i\right) \tag{17a}$$

$$\hat{\mathbf{t}} = \arg\min F(\mathbf{t}) \tag{17b}$$

where $\hat{\mathbf{t}} = (\hat{\mathbf{t}}_1^T, \hat{\mathbf{t}}_2^T, \ldots, \hat{\mathbf{t}}_k^T)^T$ is the estimated trajectory with $\hat{\mathbf{t}}_k$ being the estimated translation of the robot at time instant k.

4) Sliding Trajectory Window: Considering that the computation in cost function (17) will increase as the number of constrained equations increases, a sliding trajectory window is designed to ensure that the computation in (17) can be done real-time for some low power processors. At each time instant, we only estimate the trajectory within the sliding window instead of estimating the whole trajectory shown in Fig. 2. If the window size is set as N, only N latest translations within the sliding window $\mathbf{t}_N^k = (\mathbf{t}_{k-N+1}^T, \mathbf{t}_{k-N+2}^T, \ldots, \mathbf{t}_k^T)^T$ will be estimated. Then, the cost function (17) becomes

$$F\left(\mathbf{t}_N^k\right) = \sum_{i=k-N+1}^{k} \left(E_r^i + E_s^i\right) \tag{18a}$$

$$\hat{\mathbf{t}}_N^k = \arg\min F\left(\mathbf{t}_N^k\right) \tag{18b}$$

where $\hat{\mathbf{t}}_N^k = (\hat{\mathbf{t}}_{k-N+1}^T, \hat{\mathbf{t}}_{k-N+2}^T, \ldots, \hat{\mathbf{t}}_k^T)^T$ is the estimated trajectory in the sliding window. At time instant $k+1$, when the translation $\mathbf{t}_{k+1}$ is added to the sliding window, the translation $\mathbf{t}_{k-N+1}$ will be removed. Thus, the trajectory in the sliding window is updated as $\mathbf{t}_N^{k+1} = (\mathbf{t}_{k-N+2}^T, \mathbf{t}_{k-N+3}^T, \ldots, \mathbf{t}_{k+1}^T)^T$. Therefore, the number of constrained equations in (18) will remain as $2N$.

5) Outlier Rejection Algorithm: UWB-based localization may be trapped in NLOS scenarios that induce measurment outliers. An outlier rejection algorithm is designed to reject

Algorithm 1 Range-Only-Based Localization

Initialization:
  Received $k \geq N$ range measurements at time instant k;
  N latest translations in the sliding window $\mathbf{t}_N^k$;
  $\mathbf{t}_N^k = (\mathbf{t}_{k-N+1}^T, \mathbf{t}_{k-N+2}^T, \ldots, \mathbf{t}_k^T)^T$;
  Obtaining estimated trajectory $\hat{\mathbf{t}}_N^k$ by solving (18);
  Obtaining estimated translation $\hat{\mathbf{t}}_k$;
  $k_c = 1$;
While Received range measurement d_{k+1} at time instant $k+1$;
  If Condition (19) **do**
    Rejecting range measurement d_{k+1};
    $k = k+1$;
    $k_c = k_c + 1$;
    If $k_c > \gamma$ **do**
      Robot is trapped in extremely bad environment;
      Leaving the extremely bad environment;
      Restarting the localization;
    End
  Else
    $\mathbf{t}_N^{k+1} = (\mathbf{t}_{k-N+2}^T, \mathbf{t}_{k-N+3}^T, \ldots, \mathbf{t}_{k+1}^T)^T$ is updated;
    Adding E_r^{k+1} and E_s^{k+1} to the cost function (18);
    Removing E_r^{k-N+1} and E_s^{k-N+1} from (18);
    Obtaining the estimate $\hat{\mathbf{t}}_N^{k+1}$ by solving (18);
    Obtaining estimated translation $\hat{\mathbf{t}}_{k+1}$;
    $k = k+1$;
    $k_c = 1$;
  End
End

the outliers. The proposed outlier rejection algorithm (19) requires that the mobile robot start without measurement outliers, which is easy to be satisfied. At time instant k, assume that the trajectory estimate is $\hat{\mathbf{t}}_N^k = (\hat{\mathbf{t}}_{k-N+1}^T, \hat{\mathbf{t}}_{k-N+2}^T, \ldots, \hat{\mathbf{t}}_k^T)^T$. Then at time instant $k+1$, the robot receives a range measurement d_{k+1} from one of the fixed anchors $\mathbf{t}_a^{k+1}$. This range measurement d_{k+1} is considered as an outlier if the following condition is satisfied:

$$\left| \left\| \hat{\mathbf{t}}_k - \mathbf{t}_a^{k+1} \right\|_2 - d_{k+1} \right| > \frac{\gamma \cdot v_{\max}}{f} \tag{19}$$

where γ is the outlier rejection parameter, and f is the frequency of UWB sensor. If the inequality (19) is satisfied, the corresponding range constrained equation E_r^{k+1} and trajectory smoothness constrained equation E_s^{k+1} will not be added to the cost function (18), thus the translation $\mathbf{t}_{k+1}$ will not be estimated. On the contrary, if the inequality (19) is not satisfied, the measurement d_{k+1} will be used to localize the robot, and then the estimate $\hat{\mathbf{t}}_{k+1}$ can be obtained. The implementation of the range-only-based localization algorithm is given in Algorithm 1.

D. Range-Orientation-Based Localization

The proposed range-only-based localization algorithm in Section II-C is used to estimate the robot translation, which can accommodate other measurements to estimate the robot pose. In this section, an example for fusing orientation to estimate the robot pose is presented. In the experiments, the inertial measurement unit (IMU) [37] is used to verify this method.

1) Range Constrained Equation: The robot pose at time instant k is denoted as $\mathbf{P}_k \in \mathbb{R}^{4\times4}$, so that the robot trajectory can be denoted by $\mathbf{P} = (\mathbf{P}_1^T, \mathbf{P}_2^T, \ldots, \mathbf{P}_k^T)^T$. The range constrained equation E_r^k in (11) can be rewritten in a form of pose

$$E_r^k = w_r^k \cdot \rho\left(e_r^k\right) \tag{20a}$$

$$e_r^k = d_k - \left\| \left(\mathbf{P}_k - \mathbf{P}_a^k\right) \cdot (0,0,0,1)^T \right\|_2 \tag{20b}$$

where $\mathbf{P}_a^k$ is the anchor pose.

2) Trajectory Smoothness Constrained Equation: The trajectory smoothness constrained equation E_p^k between adjacent poses $\mathbf{P}_k$ and $\mathbf{P}_{k-1}$ is designed as

$$E_p^k = \rho\left(\sqrt{\mathbf{e}_p^{k\,T} \mathbf{w}_p^k \mathbf{e}_p^k}\right) \tag{21a}$$

$$\mathbf{e}_p^k = \mathbf{log}_{\mathrm{SE}(3)}\left(\begin{bmatrix} \breve{\mathbf{R}}_{k-1}^{-1}\breve{\mathbf{R}}_k & \mathbf{0} \\ \mathbf{0} & 1 \end{bmatrix} \cdot \mathbf{P}_k^{-1} \cdot \mathbf{P}_{k-1}\right) \tag{21b}$$

where function $\mathbf{log}_{\mathrm{SE}(3)}(\cdot)$ is defined in (3). The $\breve{\mathbf{R}}_k$ and $\breve{\mathbf{R}}_{k-1}$ are measurements from orientation sensor. $\mathbf{w}_p^k \in \mathbb{R}^{6\times6}$ is the weight designed as

$$\mathbf{w}_p^k = \mathrm{diag}(\mathbf{w}_o^k, \mathbf{w}_t^k) \tag{22}$$

where $\mathbf{w}_o^k \in \mathbb{R}^{3\times3}$ is the weight of the rotation estimate, which is provided by orientation sensor. $\mathbf{w}_t^k \in \mathbb{R}^{3\times3}$ is the weight of translation estimate designed as

$$\mathbf{w}_t^k = \mathrm{diag}(w_s^k, w_s^k, w_s^k) \tag{23}$$

where w_s^k is designed in (16). Since $\mathbf{w}_o^k$ and $\mathbf{w}_t^k$ are independent in (22), we can know that fusing the orientation information to (21) will not influence the estimation of translation. By combining (20) and (21), the trajectory in the sliding window $\mathbf{P}_N^k = (\mathbf{P}_{k-N+1}^T, \mathbf{P}_{k-N+2}^T, \ldots, \mathbf{P}_k^T)^T$ can be estimated by solving the following cost function:

$$F\left(\mathbf{P}_N^k\right) = \sum_{i=k-N+1}^{k} \left(E_r^i + E_p^i\right) \tag{24a}$$

$$\hat{\mathbf{P}}_N^k = \arg\min F\left(\mathbf{P}_N^k\right) \tag{24b}$$

where $\hat{\mathbf{P}}_N^k = (\hat{\mathbf{P}}_{k-N+1}^T, \hat{\mathbf{P}}_{k-N+2}^T, \ldots, \hat{\mathbf{P}}_k^T)^T$ is the estimated trajectory with $\hat{\mathbf{P}}_k$ being the estimated pose of the robot at time instant k.

III. Optimization

A. Optimization in Euclidean Space

For the range-only-based localization, its cost function (18) with respect to $\mathbf{t}_N^k = (\mathbf{t}_{k-N+1}^T, \mathbf{t}_{k-N+2}^T, \ldots, \mathbf{t}_k^T)^T$ is optimized in Euclidean space

$$F\left(\mathbf{t}_N^k\right) = \sum_{i=k-N+1}^{k} \phi_r^i + \phi_s^i \tag{25}$$

where

$$\begin{aligned}\phi_r^i &= w_r^i \cdot \rho\big(d_i - \left\|\mathbf{t}_i - \mathbf{t}_a^i\right\|_2\big)\\ \phi_s^i &= w_s^i \cdot \rho\big(\|\mathbf{t}_i - \mathbf{t}_{i-1}\|_2\big)\\ \rho(\cdot) &= \xi^2\left(\sqrt{1+(\cdot/\xi)^2}-1\right).\end{aligned} \tag{26}$$

The Levenberg–Marquardt [38] method is used to optimize this cost function. The initial guess of $\mathbf{t}_N^k$ is denoted by $\bar{\mathbf{t}}_N^k$, and $\Delta\mathbf{t}_N^k = \mathbf{t}_N^k - \bar{\mathbf{t}}_N^k$ is an increment. Then, we can obtain

$$F\left(\mathbf{t}_N^k\right) \simeq F\left(\bar{\mathbf{t}}_N^k\right) + \Delta\mathbf{t}_N^{k\,T} \bigtriangledown F\left(\bar{\mathbf{t}}_N^k\right) + \frac{1}{2}\Delta\mathbf{t}_N^{k\,T}\mathbf{B}_N\left(\bar{\mathbf{t}}_N^k\right)\Delta\mathbf{t}_N^k \tag{27}$$

where $\mathbf{B}_N(\bar{\mathbf{t}}_N^k)$ is a symmetric matrix that approximates the Hessian matrix $\bigtriangledown^2 F(\bar{\mathbf{t}}_N^k)$. Taking the derivative with respect to the increment $\Delta\mathbf{t}_N^k$, we have

$$\mathbf{B}_N\left(\bar{\mathbf{t}}_N^k\right)\Delta\mathbf{t}_N^k = -\bigtriangledown F\left(\bar{\mathbf{t}}_N^k\right). \tag{28}$$

Considering that the increment $\Delta\mathbf{t}_N^k$ cannot be acquired uniquely if the matrix $\mathbf{B}_N(\bar{\mathbf{t}}_N^k)$ is singular, the Levenberg–Marquardt method introduces a damping factor $\lambda_k > 0$ to solve this problem

$$\left(\mathbf{B}_N\left(\bar{\mathbf{t}}_N^k\right) + \lambda_k\mathbf{I}\right)\Delta\mathbf{t}_N^k = -\bigtriangledown F\left(\bar{\mathbf{t}}_N^k\right) \tag{29}$$

where $\mathbf{I}$ is identity matrix. The estimate $\hat{\mathbf{t}}_N^k$ is obtained by

$$\hat{\mathbf{t}}_N^k = \bar{\mathbf{t}}_N^k + \Delta\mathbf{t}_N^k, \quad \bar{\mathbf{t}}_N^k = \hat{\mathbf{t}}_N^k. \tag{30}$$

The optimization process (27)–(30) continues until the number of iterations is reached or the value of cost function is smaller than a threshold.

B. Optimization in Non-Euclidean Space

For fusing the orientation to estimate the robot pose, the corresponding cost function (24) is optimized in non-Euclidean space. To solve (24), an idea is to map the cost function (24) into Euclidean space by a mapping function (3). The pose $\mathbf{P}_k$ can be represented by its corresponding vector $\epsilon_k \in \mathbb{R}^6$, so that the cost function (24) can be rewritten as

$$F\left(\epsilon_N^k\right) = \sum_{i=k-N+1}^{k}\left(E_r^i + E_p^i\right) \tag{31a}$$

$$\hat{\epsilon}_N^k = \arg\min F\left(\epsilon_N^k\right) \tag{31b}$$

where $\epsilon_N^k = (\epsilon_{k-N+1}^T, \epsilon_{k-N+2}^T, \ldots, \epsilon_k^T)^T$. Similar to the process (27)–(30), the estimate $\hat{\epsilon}_N^k = (\hat{\epsilon}_{k-N+1}^T, \hat{\epsilon}_{k-N+2}^T, \ldots, \hat{\epsilon}_k^T)^T$ can be obtained. Then, the estimated trajectory $\hat{\mathbf{P}}_N^k = (\hat{\mathbf{P}}_{k-N+1}^T, \hat{\mathbf{P}}_{k-N+2}^T, \ldots, \hat{\mathbf{P}}_k^T)^T$ can be acquired by (3).

C. Computational Complexity

Observe that the computational complexity of the proposed range-only-based algorithm and range-orientation-based algorithm is dominated by (27)–(30). Suppose that M is the number of iterations used for Levenberg–Marquardt method and N is the size of the sliding window. The matrix inverse calculation is involved and its complexity is around $O(N^3)$ [39]. Hence, the computational upper bound of optimization in (27)–(30) is $O(MN^3)$. Fortunately, the matrix $\mathbf{B}_N + \lambda\mathbf{I}$ in (29) is sparse if $N > 5$, i.e., only $9(3N-2)$ entries are nonzero. By taking advantage of this characteristic of $\mathbf{B}_N + \lambda\mathbf{I}$, the increment $\Delta\mathbf{t}_N^k$ in (30) can be calculated efficiently by the sparse Cholesky factorization algorithm [40]. When the window size is set as $N = 10$ and the number of iterations is taken as $M = 10$, the corresponding running time of the proposed algorithm in different power processors is shown in Table II. Note that if the update rate (reciprocal of running time) of the proposed algorithm is lower than the frequency of the UWB sensor, the proposed algorithm will lose some range measurements, resulting in a larger translation estimation error. The frequency of the UWB sensor in our experiments is 32.46 Hz. Hence, the maximum allowed running time is $1/32.46 \simeq 0.0308$ s. It can be seen from Table II that the proposed method can be applied in some low power processors, such as Intel Atom x7-Z8750 and Quad-core ARM Cortex-A53 for localization because they can run the proposed algorithm in less than 0.0308 s.

TABLE II
RUNNING TIME OF THE PROPOSED ALGORITHM IN DIFFERENT POWER PROCESSORS WITH $M = 10$ AND $N = 10$

Processors	Running time (s)
Intel core i7 processor	0.0019
Intel Atom x7-Z8750 processor	0.0057
Quad-core ARM Cortex-A53 processor	0.0301

IV. STABILITY ANALYSIS

For the range-only-based cost function (25), the performance of the iterative algorithms (30) will be analyzed. For the range measurements $d_N^k = (d_{k-N+1}, d_{k-N+2}, \ldots, d_k)$ and $\mathbf{t}_N^k = (\mathbf{t}_{k-N+1}^T, \mathbf{t}_{k-N+2}^T, \ldots, \mathbf{t}_k^T)^T$ is the corresponding trajectory in the sliding window. The translation $\mathbf{t}_i = \mathbf{A}_i \cdot \mathbf{t}_N^k$ can be extracted from $\mathbf{t}_N^k$ by a matrix $\mathbf{A}_i \in \mathbb{R}^{3\times 3N}$. $\bar{\mathbf{t}}_N^k = (\bar{\mathbf{t}}_{k-N+1}^T, \bar{\mathbf{t}}_{k-N+2}^T, \ldots, \bar{\mathbf{t}}_k^T)^T$ is the initial guess of $\mathbf{t}_N^k$. Then, the gradient and Hessian of the cost function (25) with respect to the initial guess $\bar{\mathbf{t}}_N^k$ are

$$\begin{aligned}\bigtriangledown F\left(\bar{\mathbf{t}}_N^k\right) = &-\sum_{i=k-N+1}^{k}\mathbf{A}_i^T \cdot y_i\left(\bar{\mathbf{t}}_i\right)\cdot w_r^i \cdot \bigtriangledown\mathbf{h}_i\left(\bar{\mathbf{t}}_i\right)\\ &+\sum_{i=k-N+2}^{k}\left(\mathbf{A}_i^T - \mathbf{A}_{i-1}^T\right)\cdot \mathbf{z}_i\left(\bar{\mathbf{t}}_i - \bar{\mathbf{t}}_{i-1}\right)\\ &\times w_s^i + \chi_{k-N+1}\end{aligned} \tag{32}$$

where

$$\begin{aligned}m_i\left(\bar{\mathbf{t}}_i\right) &= d_i - \left\|\bar{\mathbf{t}}_i - \mathbf{t}_a^i\right\|_2\\ y_i\left(\bar{\mathbf{t}}_i\right) &= \frac{m_i\left(\bar{\mathbf{t}}_i\right)}{\sqrt{1+\frac{m_i^2\left(\bar{\mathbf{t}}_i\right)}{\xi^2}}}\\ \bigtriangledown\mathbf{h}_i\left(\bar{\mathbf{t}}_i\right) &= \frac{\bar{\mathbf{t}}_i - \mathbf{t}_a^i}{\left\|\bar{\mathbf{t}}_i - \mathbf{t}_a^i\right\|_2}\end{aligned}$$

$$\mathbf{z}_i\left(\bar{\mathbf{t}}_i-\bar{\mathbf{t}}_{i-1}\right)=\frac{\bar{\mathbf{t}}_i-\bar{\mathbf{t}}_{i-1}}{\sqrt{1+\frac{\left\|\bar{\mathbf{t}}_i-\bar{\mathbf{t}}_{i-1}\right\|_2^2}{\xi^2}}}$$
$$\chi_{k-N+1}=\mathbf{A}_{k-N+1}^T\cdot\frac{\bar{\mathbf{t}}_{k-N+1}-\hat{\mathbf{t}}_{k-N}}{\sqrt{1+\frac{\left\|\bar{\mathbf{t}}_{k-N+1}-\hat{\mathbf{t}}_{k-N}\right\|_2^2}{\xi^2}}}\cdot w_s^{k-N+1}. \tag{33}$$

The $\hat{\mathbf{t}}_{k-N}$ in (33) is from the estimate $\hat{\mathbf{t}}_N^{k-1}$, and

$$\begin{aligned}\bigtriangledown^2 F\left(\bar{\mathbf{t}}_N^k\right)=&-\sum_{i=k-N+1}^{k}\mathbf{A}_i^T\cdot w_r^i\cdot\mathbf{s}_i\left(\bar{\mathbf{t}}_i\right)\cdot\mathbf{A}_i\\&+\sum_{i=k-N+2}^{k}\left(\mathbf{A}_i^T-\mathbf{A}_{i-1}^T\right)\cdot\mathbf{x}_i\left(\bar{\mathbf{t}}_i-\bar{\mathbf{t}}_{i-1}\right)\\&\times w_s^i\cdot\left(\mathbf{A}_i-\mathbf{A}_{i-1}\right)\\&+\mathbf{A}_{k-N+1}^T\cdot\varpi_{k-N+1}\cdot w_s^{k-N+1}\cdot\mathbf{A}_{k-N+1}\end{aligned} \tag{34}$$

where

$$\begin{aligned}\mathbf{s}_i\left(\bar{\mathbf{t}}_i\right)&=\bigtriangledown\mathbf{y}_i\left(\bar{\mathbf{t}}_i\right)\cdot\bigtriangledown\mathbf{h}_i^T\left(\bar{\mathbf{t}}_i\right)+y_i\left(\bar{\mathbf{t}}_i\right)\cdot\bigtriangledown^2\mathbf{h}_i\left(\bar{\mathbf{t}}_i\right)\\\bigtriangledown\mathbf{y}_i\left(\bar{\mathbf{t}}_i\right)&=-l_i\left(\bar{\mathbf{t}}_i\right)\cdot\bigtriangledown\mathbf{h}_i\left(\bar{\mathbf{t}}_i\right)\\l_i\left(\bar{\mathbf{t}}_i\right)&=\frac{1}{\left(1+\frac{m_i^2\left(\bar{\mathbf{t}}_i\right)}{\xi^2}\right)^{\frac{3}{2}}}\\\bigtriangledown^2\mathbf{h}_i\left(\bar{\mathbf{t}}_i\right)&=\frac{\mathbf{I}-\bigtriangledown\mathbf{h}_i\left(\bar{\mathbf{t}}_i\right)\cdot\bigtriangledown\mathbf{h}_i^T\left(\bar{\mathbf{t}}_i\right)}{\left\|\mathbf{t}_i-\mathbf{t}_a^i\right\|_2}\\\mathbf{x}_i\left(\bar{\mathbf{t}}_i-\bar{\mathbf{t}}_{i-1}\right)&=\frac{\left(\xi^2+\left\|\bar{\mathbf{t}}_i-\bar{\mathbf{t}}_{i-1}\right\|_2^2\right)\mathbf{I}-\left(\bar{\mathbf{t}}_i-\bar{\mathbf{t}}_{i-1}\right)\left(\bar{\mathbf{t}}_i-\bar{\mathbf{t}}_{i-1}\right)^T}{\xi^2\left(1+\frac{\left\|\bar{\mathbf{t}}_i-\bar{\mathbf{t}}_{i-1}\right\|_2^2}{\xi^2}\right)^{\frac{3}{2}}}\\\varpi_{k-N+1}&=\frac{\left(\xi^2+\left\|\bar{\mathbf{t}}_{k-N+1}-\hat{\mathbf{t}}_{k-N}\right\|_2^2\right)\mathbf{I}-\left(\bar{\mathbf{t}}_{k-N+1}-\hat{\mathbf{t}}_{k-N}\right)\left(\bar{\mathbf{t}}_{k-N+1}-\hat{\mathbf{t}}_{k-N}\right)^T}{\xi^2\left(1+\frac{\left\|\bar{\mathbf{t}}_{k-N+1}-\hat{\mathbf{t}}_{k-N}\right\|_2^2}{\xi^2}\right)^{\frac{3}{2}}}.\end{aligned} \tag{35}$$

From (10) and (14), we can know that $\mathbf{t}_N^k$ belongs to the set X_N^k

$$\begin{aligned}X_N^k=\Big\{&\mathbf{t}_N^k:\left\|\mathbf{t}_i-\mathbf{t}_a^i\right\|_2\le d_i+\eta,\left\|\mathbf{t}_i-\mathbf{t}_{i-1}\right\|_2\le v_{\max}\cdot T_N^k\\&T_N^k=\max(\Delta T_{k-N+1},\Delta T_{k-N+2},\ldots,\Delta T_k)\\&i=k-N+2,k-N+3,\ldots,k\Big\}.\end{aligned} \tag{36}$$

For the Hessian matrix, let

$$\delta_s^k=\min_{\left\{\mathbf{t}_N^k\in X_N^k,\theta\in[0,1]\right\}}\left\|\bigtriangledown^2F\left(\theta\mathbf{t}_N^k+(1-\theta)\bar{\mathbf{t}}_N^k\right)\right\|_2 \tag{37}$$

and

$$\delta_l^k=\max_{\left\{\mathbf{t}_N^k\in X_N^k,\theta\in[0,1]\right\}}\left\|\bigtriangledown^2F\left(\theta\mathbf{t}_N^k+(1-\theta)\bar{\mathbf{t}}_N^k\right)\right\|_2. \tag{38}$$

Also, let

$$\mu_N^k=\left\|\mathbf{B}_N\left(\bar{\mathbf{t}}_N^k\right)+\lambda_k\mathbf{I}\right\|_2 \tag{39}$$

where $\mathbf{B}_N(\bar{\mathbf{t}}_N^k)$ is from (27). Inspired by the work [14], define stability parameter α_k as

$$\alpha_k=\max\left(\left|1-\frac{\delta_s^k}{\mu_N^k}\right|,\left|1-\frac{\delta_l^k}{\mu_N^k}\right|\right). \tag{40}$$

The stability parameter α_k plays a crucial role in ensuring the convergence of the proposed method.

Theorem 1: Suppose stability parameter (40) satisfies $\alpha_i<1$, $(i=N+1,N+2,\ldots,k+1)$. Then, the trajectory estimation error for the range-only-based cost function (25) given by the Levenberg–Marquardt method is bounded if the range measurement noise is bounded.

Proof: The initial guess $\bar{\mathbf{t}}_N^{k+1}$ of $\mathbf{t}_N^{k+1}$ is set as $\bar{\mathbf{t}}_N^{k+1}=\hat{\mathbf{t}}_N^k$. The estimate $\hat{\mathbf{t}}_N^{k+1}$ based on the (29) and (30) with single iteration is

$$\hat{\mathbf{t}}_N^{k+1}=\bar{\mathbf{t}}_N^{k+1}-\left(\mathbf{B}_N\left(\bar{\mathbf{t}}_N^{k+1}\right)+\lambda_{k+1}\mathbf{I}\right)^{-1}\bigtriangledown F\left(\bar{\mathbf{t}}_N^{k+1}\right). \tag{41}$$

According to the mean value theorem, it follows that there exists $\theta\in[0,1]$ such that:

$$\begin{aligned}\bigtriangledown F\left(\bar{\mathbf{t}}_N^{k+1}\right)=&\bigtriangledown F\left(\mathbf{t}_N^{k+1}\right)\\&+\bigtriangledown^2F\left(\theta\mathbf{t}_N^{k+1}+(1-\theta)\bar{\mathbf{t}}_N^{k+1}\right)\left(\bar{\mathbf{t}}_N^{k+1}-\mathbf{t}_N^{k+1}\right).\end{aligned} \tag{42}$$

Then, combining (32) and (10), it yields

$$\begin{aligned}\bigtriangledown F\left(\bar{\mathbf{t}}_N^{k+1}\right)=&\eta_N^{k+1}\\&+\bigtriangledown^2F\left(\theta\mathbf{t}_N^{k+1}+(1-\theta)\bar{\mathbf{t}}_N^{k+1}\right)\left(\bar{\mathbf{t}}_N^{k+1}-\mathbf{t}_N^{k+1}\right)\end{aligned} \tag{43}$$

where

$$\begin{aligned}\eta_N^{k+1}=&-\sum_{i=k-N+2}^{k+1}\mathbf{A}_i^T\cdot y_i(\mathbf{t}_i)\cdot w_r^i\cdot\bigtriangledown\mathbf{h}_i(\mathbf{t}_i)\\&+\sum_{i=k-N+3}^{k+1}\left(\mathbf{A}_i^T-\mathbf{A}_{i-1}^T\right)\cdot\mathbf{z}_i(\mathbf{t}_i-\mathbf{t}_{i-1})\cdot w_s^i+\chi_{k-N+2}.\end{aligned} \tag{44}$$

From (12) and (33), we have

$$\begin{aligned}&y_i(\cdot)<\xi,\left\|\mathbf{z}_i(\cdot)\right\|_2<\xi,\left\|w_r^i\right\|_2<1,\left\|w_s^i\right\|_2<1\\&\left\|\bigtriangledown\mathbf{h}_i(\cdot)\right\|_2=1,\left\|\mathbf{A}_i\right\|_2\le1,\left\|\mathbf{A}_i-\mathbf{A}_{i-1}\right\|_2\le2\\&\left\|\chi_{k-N+2}\right\|_2\le\xi.\end{aligned} \tag{45}$$

Then, it yields

$$\left\|\eta_N^{k+1}\right\|_2<N\xi+2(N-1)\xi+\xi\le(3N-1)\xi. \tag{46}$$

Let trajectory estimation error be $\mathbf{e}_{k+1}=\hat{\mathbf{t}}_N^{k+1}-\mathbf{t}_N^{k+1}$. $\mathbf{r}_N^{k+1}=(\mathbf{r}_{k-N+2}^T,\mathbf{r}_{k-N+3}^T,\ldots,\mathbf{r}_{k+1}^T)^T$ is the unknown relative translations with $\|\mathbf{r}_N^{k+1}\|_2\le N\cdot v_{\max}\cdot T_N^{k+1}$. We have $\bar{\mathbf{t}}_N^{k+1}-\mathbf{t}_N^{k+1}=\hat{\mathbf{t}}_N^k-\mathbf{t}_N^k-\mathbf{r}_N^{k+1}=\mathbf{e}_k-\mathbf{r}_N^{k+1}$.

Combining (41) with (43) leads to

$$\begin{aligned}\mathbf{e}_{k+1}=&\bar{\mathbf{t}}_N^{k+1}-\mathbf{t}_N^{k+1}-\left(\mathbf{B}_N\left(\bar{\mathbf{t}}_N^{k+1}\right)+\lambda_{k+1}\mathbf{I}\right)^{-1}\bigtriangledown F\left(\bar{\mathbf{t}}_N^{k+1}\right)\\=&-\left(\mathbf{B}_N\left(\bar{\mathbf{t}}_N^{k+1}\right)+\lambda_{k+1}\mathbf{I}\right)^{-1}\eta_N^{k+1}+\left(\mathbf{e}_k-\mathbf{r}_N^{k+1}\right)\\&\times\left(1-\left(\mathbf{B}_N(\bar{\mathbf{t}}_N^{k+1})+\lambda_{k+1}\mathbf{I}\right)^{-1}\right.\\&\left.\times\bigtriangledown^2F\left(\theta\mathbf{t}_N^{k+1}+(1-\theta)\bar{\mathbf{t}}_N^{k+1}\right)\right).\end{aligned} \tag{47}$$

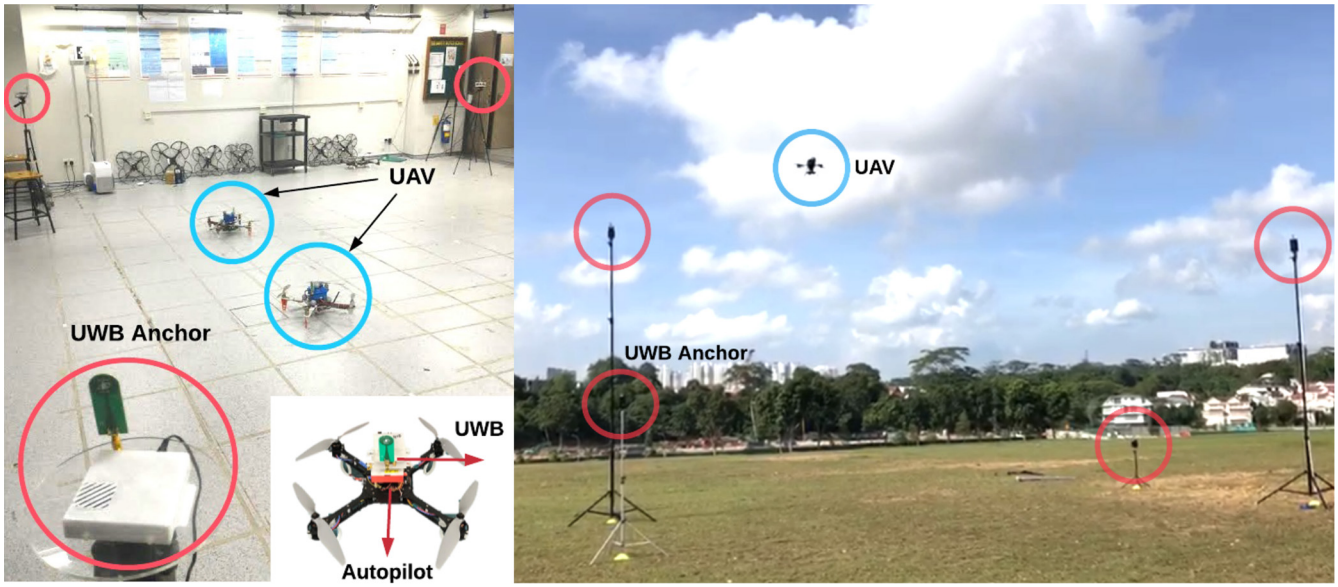

Fig. 3. Experiments are carried out in both indoor and outdoor environments. The localization system in the experiments consists of only four fixed anchors. The UAV can send requests to four fixed UWB anchors sequentially to get the range measurements.

Therefore

$$\|\mathbf{e}_{k+1}\|_2 \le \frac{\left\|\eta_N^{k+1}\right\|_2}{\mu_N^{k+1}} + \max\left(\left|1-\frac{\delta_s^{k+1}}{\mu_N^{k+1}}\right|, \left|1-\frac{\delta_l^{k+1}}{\mu_N^{k+1}}\right|\right) \times \left(\|\mathbf{e}_k\|_2 + \left\|\mathbf{r}_N^{k+1}\right\|_2\right). \tag{48}$$

Let

$$\begin{aligned} \alpha_i &= \max\left(\left|1-\frac{\delta_s^i}{\mu_N^i}\right|, \left|1-\frac{\delta_l^i}{\mu_N^i}\right|\right), \beta_i = \frac{\|\eta_N^i\|_2}{\mu_N^i} \\ c_i &= N \cdot v_{\max} \cdot T_N^i \quad (i = N+1, N+2, \ldots, k+1) \\ \alpha &= \max(\alpha_{N+1}, \alpha_{N+2}, \ldots, \alpha_{k+1}) \\ \beta &= \max(\beta_{N+1}, \beta_{N+2}, \ldots, \beta_{k+1}) \\ c &= \max(c_{N+1}, c_{N+2}, \ldots, c_{k+1}). \end{aligned} \tag{49}$$

Then, we have

$$\|\mathbf{e}_{k+1}\|_2 \le \alpha^{k-N+1}\|\mathbf{e}_N\|_2 + \sum_{i=0}^{k-N}\alpha^i\beta + \sum_{i=0}^{k-N}\alpha^{i+1}c. \tag{50}$$

If condition $\alpha_i < 1, (i = N+1, N+2, \ldots, k+1)$ holds and the range measurement noise is bounded, we get

$$\lim_{k\to\infty}\|\mathbf{e}_{k+1}\|_2 \le \frac{\beta}{1-\alpha} + \frac{\alpha c}{1-\alpha}. \tag{51}$$

The above single iteration result can be extended to multi-iteration scheme. For multi-iteration scheme, it is easy to prove that the trajectory estimation error is also bounded if the range measurement noise is bounded and $\alpha_i < 1, (i = N+1, N+2, \ldots, k+1)$. ■

Remark 4: The proposed method does not require an accurate initial guess. The parameter λ_k in (39) can be adjusted to ensure $\alpha_k < 1$ (40). Although the convergence of the cost function (25) can be guaranteed by choosing suitable parameter λ_k, we can not guarantee that there exists a unique solution to the cost function (25) because the cost function (25) is a nonconvex function. From our experiment experience, the local minimum is more likely to be avoided by setting a larger window size N.

Since $\mathbf{w}_o^k$ and $\mathbf{w}_t^k$ are independent in (22), we can know that fusing the orientation information to the proposed framework will not influence the convergence of the translation estimation.

V. Experimental Results

In this section, we use a UAV to test the performance of the proposed range-only-based and range-orientation-based localization algorithms. The hardware, experiment setup, evaluation, parameter selection, comparison of localization accuracy, the effects of different number of iterations and window size in the optimization on the localization accuracy, analysis of robust, and smoothness of the proposed algorithm are presented, respectively.

A. Hardware

Quadrotor UAV consists of four rotors that are configured in a cross shape as shown in Fig. 3. The UAV is equipped with the UWB module, IMU sensor and Pixhawk Autopilot. The UWB platform for the experiment is from time domain with operating band from 3.1 GHz to 5.3 GHz shown in Fig. 3. Within the range of 100 m, it is able to provide precise measurement at an update rate of around 40 Hz. Its dimension (7.6 cm × 8.0 cm × 1.6 cm) and weight (58 g) are suitable for micro UAVs. Our UWB ranging algorithm uses two-way TOA measurement to calculate the range shown in (10), which is able to provide relatively steady range measurements and has the ranging area of 100 m with ranging error within $\eta = 0.2$ m. The IMU sensor is from myAHRS+ (altitude heading reference system), which is a low cost high performance attitude and heading reference system (AHRS) containing a 3-axis 16-bit gyroscope, a 3-axis 16-bit accelerometer, and a 3-axis 13-bit magnetometer.

TABLE III
COMPARISON OF EXISTING RANGE-BASED LOCALIZATION METHODS IN 2-D PLANE

2-D plane	Proposed range-only based Method	MHE	UKF	EKF	NR	Particle Filter	GRNN	BPNN	KNN
Translation Error (m)	**0.031**	0.078	0.091	0.102	0.154	0.115	0.114	0.128	0.166

Best result is highlighted in black boldface. The **RMSE** of the proposed method in 2-D plane is **0.033**m.
The range-only based localization and range-orientation based localization achieved the same localization accuracy in translation.
GRNN: Generalized regression neural network, **BPNN**: Back propagation neural network, **KNN**: K-nearest neighbor method.

B. Experiment Setup and Evaluation

The indoor experiments were carried out in an area of 6 m × 6 m × 3 m, and outdoor experiments were carried out within an area of 6 m × 8 m × 5 m. The four noncoplanar fixed anchors are used in our experiments. UAV will send requests to four fixed UWB anchors sequentially to get the range measurements. The ground truth is provided by a VICON system which has a localization accuracy of mm-level. In order to analyze the localization accuracy, the mean error E_T and root mean square error E_{RMSE} of translation are given by

$$E_T = \frac{1}{k}\sum_{i=1}^{k}\left\|\hat{\mathbf{t}}_i - \mathbf{t}_i\right\|_2 \tag{52}$$

$$E_{\text{RMSE}} = \sqrt{\frac{1}{k}\sum_{i=1}^{k}\left\|\hat{\mathbf{t}}_i - \mathbf{t}_i\right\|_2^2} \tag{53}$$

where $\hat{\mathbf{t}}_i$ and $\mathbf{t}_i$ are the estimate and ground truth, respectively.

The mean error of rotation E_O is given by

$$E_O = \frac{1}{k}\sum_{i=1}^{k}\left\|\hat{\mathbf{R}}_i\mathbf{R}_i^{-1} - \mathbf{I}\right\| \tag{54}$$

where $\hat{\mathbf{R}}_i$ is the estimated rotation, and $\mathbf{R}_i$ is the rotation from the orientation sensor.

Since IMU and UWB measurements may not be obtained at the same time instant, a time synchronizer filter is used to synchronize incoming IMU and UWB measurements. At each time instant when a UWB measurement is received, we get a ranging measurement for constructing range constrained (20), then IMU measurement whose time instant is closest to the incoming UWB time instant is chosen for constructing trajectory smoothness constrained (21). Since the IMU has a much higher data rate, the remaining IMU measurements are not used.

C. Parameter Selection

To implement the proposed method, the system parameters need to be tuned.

1) Known Parameters: These parameters are determined by the experiment area and hardware shown as follows.

1) Anchor translations $\mathbf{t}_a^k$ in (11) in door environments are $(3, 3, 1.95)$, $(3, -3, 0.53)$, $(-3, 3, 0.54)$, and $(-3, -3, 1.98)$, respectively, and $(0, 0, 0.79)$, $(6, 0, 5)$, $(6, 8, 1.52)$, and $(0, 8, 5.52)$ in outdoor environments. The unit is metre(m).
2) Range measurement d_k in (11) is from UWB sensor.
3) The upper bound of range measurement noise is $\eta = 0.2$ m.

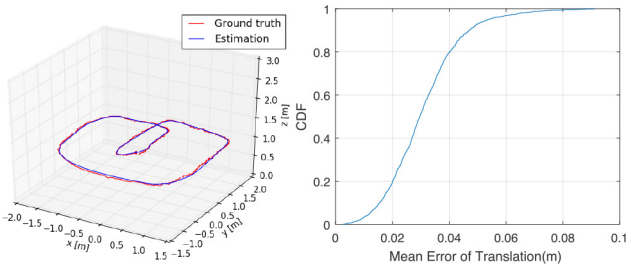

Fig. 4. UAV moved along a circle or rectangle in a 2-D plane. In the left figure, the red line is ground truth from VICON system, and the blue line is the range-only-based estimation. The cumulative distribution of mean error of translation is presented in the right figure.

4) Frequency of UWB sensor in (19) is $f = 32.46$ Hz.
5) Frequency of IMU sensor is 100.3 Hz.

2) Tuning Parameters: These parameters are tuned according to different experiment environment. In our experiments, these parameters are set as follows.

1) The variance of range measurement noise in (12) is set as $\sigma_r^2 = (\eta^2/9)$.
2) The selections of the weights w_s^k and $\mathbf{w}_t^k$ are presented in (16) and (23).
3) The initial guess of robot rotation $\mathbf{R}_k$ in $\mathbf{P}_k$ is set as $\breve{\mathbf{R}}_k$, where $\breve{\mathbf{R}}_k$ is the IMU measurement. The initial guess of robot translation is set randomly.

D. Comparison With Existing Range-Based Localization Methods

The UAV moved along a circle or a rectangle in our experiments. The range-only-based localization (18) and range-orientation-based localization (24) obtained similar localization accuracy in translation, which verified that fusing the orientation information to the proposed framework will not influence the estimation of translation. For the range-orientation-based localization (24), the mean error of rotation in (54) is only 0.0023.

For the comparison with existing methods [UKF, EKF, nonlinear regression (NR), MDS, and RVFL] [11], [17], [22], [23], we implemented their algorithms in the same environment of our lab with the best choices of parameters to ensure the fairness of the comparison. The results of MHE and particle filter method are from [32], [36], and [41]. We adopted the experimental results of the machine learning methods (GRNN, BPNN, and KNN) in the latest work [42].

We conduct more than 50 experiments in a two-dimensional (2-D) plane, in which one of the examples is shown in Fig. 4, where the cumulative distribution (CDF) of mean error of translation is presented, and the ground truth and estimated

TABLE IV
COMPARISON OF EXISTING RANGE-BASED LOCALIZATION METHODS IN 3-D SPACE

3-D space	Proposed range-only based Method	UKF	EKF	NR	RVFL+FS	MDS+PSO	MHE
Mean Error of x (m)	**0.023**	0.062	0.114	0.102	-	-	-
Mean Error of y (m)	**0.022**	0.066	0.123	0.116	-	-	-
Mean Error of z (m)	**0.077**	**0.232**	**0.353**	**0.346**	-	-	-
Translation Error (m)	**0.083**	**0.249**	**0.391**	**0.379**	**0.340**	**0.698**	**>1**

Best results are highlighted in black boldface. The **RMSE** of the proposed method in 3-D space is **0.081**m.
Weak results in the existing range-based localization methods are highlighted in red boldface.
The range-only based localization and range-orientation based localization achieved the same localization accuracy in translation.
PSO: Particle swarm optimization, **RVFL**: Random vector functional link network, **FS**: Feature Selection.

trajectory are shown in red and blue lines, respectively. The mean error and root mean square error of translation of the proposed method are 3.1 and 3.3 cm, respectively. The CDF of mean error of translation in 2-D plane shows that about 75 percent of translation errors are within 4 cm. In comparison with other range-based localization methods in 2-D plane, the localization accuracy of the proposed algorithm has improved more than 3 times as shown in Table III.

Similarly, Fig. 5. shows one of the experiments conducted in 3-D space. The mean error and root mean square error of translation of the proposed method are 8.3 and 8.1 cm, respectively. The CDF of mean error of translation in 3-D space shows that about 75 percent of translation errors are within 8 cm. The comparison with other range-based localization methods in 3-D space is shown in Table IV. The localization accuracy in x or y direction has improved more than 3 times. The mean errors of the existing methods are about 6.2 to 12.3 cm in the x and y directions. But the mean errors of our proposed algorithm are about 2.3 and 2.2 cm in the x and y directions, which are much more accurate than the existing methods.

Compared with existing experimental results, it is worth noting that the localization accuracy in the altitude improved greatly without the need of adding altitude sensors to measure the altitude or placing the anchors on the ceiling. The mean error in the z direction is about 7.7 cm, which is accurate enough to fly a UAV in 3-D space as demonstrated in our UAV flight experiment.

Remark 5: As the ground truth of the mobile robot is obtained by a VICON system which is limited to an area of 6 m $\times$ 6 m $\times$ 3 m, we can only compare the proposed method with others within the area of 6 m $\times$ 6 m $\times$ 3 m. It is worth noting that the proposed general framework was also successfully applied in the UWB-aided visual SLAM with an improved performance [28].

E. Effects of the Number of Iterations and Window Size

There are two important tuning parameters needed to be analyzed. One is the number of iterations M, and the other is the window size N. The effects of the different number of iterations and window size in the optimization on localization accuracy are analyzed on 2.2 GHz intel core i7 processor. The mean error of translation of the proposed method with the different number of iterations and window size in both 2-D plane and 3-D space are shown in Fig. 6. When $N > 5$ and $M \cdot N < 2000$, good localization accuracy can be obtained.

It is intuitive that if the update rate of the proposed algorithm (reciprocal of running time) is lower than the frequency

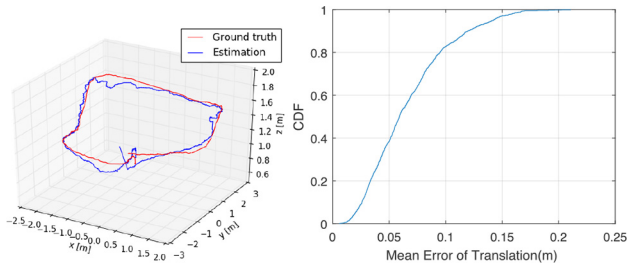

Fig. 5. UAV moved in a 3-D space. In the left figure, the red line is ground truth from VICON system, and the blue line is the range-only-based estimation. The cumulative distribution of mean error of translation is presented in the right figure.

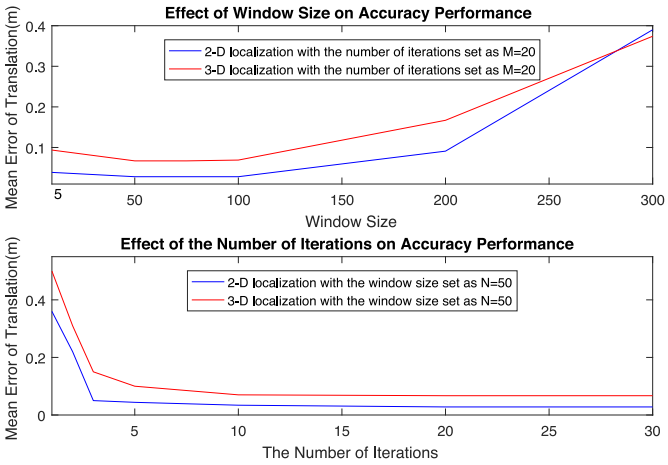

Fig. 6. Effects of different iteration number and window size on mean translation error.

of the UWB sensor, the proposed algorithm will lose some range measurements, resulting in a larger translation estimation error. To guarantee a good performance of the proposed method on different power processors and scenarios, the following two conditions should be satisfied.

1) The mobile robot can receive the range measurements from at least four noncoplanar anchors.
2) The number of iterations and window size should be adjusted to ensure that the update rate of the proposed algorithm is larger than the frequency of the range sensor.

F. Robust: Outlier Rejection

An outlier rejection test with four fixed UWB anchors and a static robot is presented. The range measurements from the four anchors should be almost constant if there is no

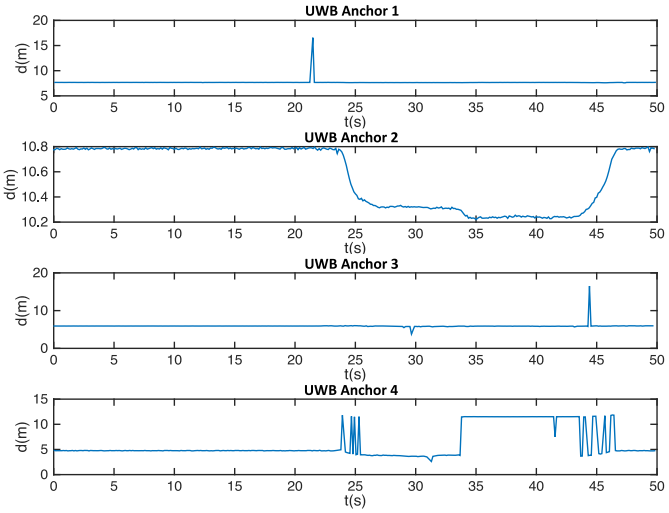

Fig. 7. Existence of outliers in the measurements.

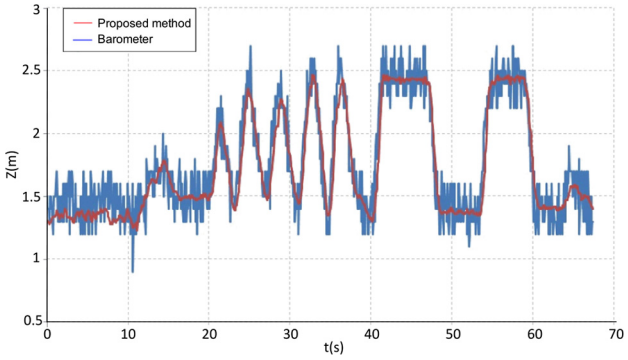

Fig. 8. Comparison between barometer sensor (blue line) and our method (red line) in estimating altitude.

NLOS measurement. In this test, UWB anchors have outliers, which are rejected based on the algorithm (19). Our method can still provide stable translation estimation even if the outliers exist for seconds. For example, UWB Anchor 4 has outliers from 23.7 s to 25.4 s and 33.8 s to 47.3 s, respectively shown in Fig. 7. The translations of four fixed UWB anchors are $(0, 0, 0.77)$, $(6.13, 0, 5)$, $(6.01, 8.07, 0.79)$, and $(0.11, 8.02, 5.02)$, respectively. The test result showed that we can get accurate translation estimation $(0.14, 7.63, 0.29)$, which is close to the ground truth $(0.12, 7.61, 0.23)$ during the whole 50 s, which verifies the robust of the proposed method.

G. Smoothness: Comparison With Barometer Sensor

We have verified that the proposed method obtains high localization accuracy in the altitude. In addition, we find that the proposed method performs better on smoothness than the barometer. It can be seen from Fig. 8 that barometer reading is noisy, but our proposed method is smooth due to the design of trajectory smoothness constrained equation between adjacent translations.

VI. Conclusion

In this article, a general graph optimization-based localization framework was proposed that allows the fusion of various sensor measurements for localization. Special emphasis was then given to the range-based localization, which removes the dependence on the kinematic model and requirement of receiving multiple range measurements concurrently, and can be implemented real-time in some low power systems. Compared with existing range-based localization methods, better localization accuracy in both 2-D plane and 3-D space were obtained, especially in the altitude direction.

References

[1] S. Minaeian, J. Liu, and Y.-J. Son, "Vision-based target detection and localization via a team of cooperative UAV and UGVs," *IEEE Trans. Syst., Man, Cybern., Syst.*, vol. 46, no. 7, pp. 1005–1016, Jul. 2016.

[2] Z. Wu, Q. Xu, J. Li, C. Fu, Q. Xuan, and Y. Xiang, "Passive indoor localization based on CSI and Naive Bayes classification," *IEEE Trans. Syst., Man, Cybern., Syst.*, vol. 48, no. 9, pp. 1566–1577, Sep. 2018.

[3] C. Wang, J. Yuan, and L. Xie, "Non-iterative SLAM," in *Proc. 18th Int. Conf. Adv. Robot. (ICAR)*, 2017, pp. 83–90.

[4] C. Wang, L. Zhang, L. Xie, and J. Yuan, "Kernel cross-correlator," in *Proc. 32nd AAAI Conf. Artif. Intell.*, 2018, pp. 4179–4186.

[5] B. Zhu, L. Xie, D. Han, X. Meng, and R. Teo, "A survey on recent progress in control of swarm systems," *Sci. China Inf. Sci.*, vol. 60, no. 7, pp. 1–24, 2017.

[6] J. Li, Z. Wang, Y. Shen, and Y. Wang, "Interval observer design for discrete-time uncertain Takagi–Sugeno fuzzy systems," *IEEE Trans. Fuzzy Syst.*, vol. 27, no. 4, pp. 816–823, Apr. 2019.

[7] E. Jakob, S. Thomas, and C. Daniel, "LSD-SLAM: Large-scale direct monocular SLAM," in *Proc. Eur. Conf. Comput. Vis.*, 2014, pp. 834–849.

[8] Z. Chen, H. Zou, H. Jiang, Q. Zhu, Y. Soh, and L. Xie, "Fusion of Wi-Fi, smartphone sensors and landmarks using the Kalman filter for indoor localization," *Sensors*, vol. 15, no. 1, pp. 715–732, 2015.

[9] S. Lupashin, M. Hehn, M. W. Mueller, A. P. Schoellig, M. Sherback, and R. DAndrea, "A platform for aerial robotics research and demonstration: The flying machine arena," *Mechatronics*, vol. 24, no. 1, pp. 41–54, 2014.

[10] S. Zihajehzadeh and E. J. Park, "A novel biomechanical model-aided IMU/UWB fusion for magnetometer-free lower body motion capture," *IEEE Trans. Syst., Man, Cybern., Syst.*, vol. 47, no. 6, pp. 927–938, Jun. 2017.

[11] W. Cui, C. Wu, W. Meng, B. Li, Y. Zhang, and L. Xie, "Dynamic multidimensional scaling algorithm for 3-D mobile localization," *IEEE Trans. Instrum. Meas.*, vol. 65, no. 12, pp. 2853–2865, Dec. 2016.

[12] Y. Shang and W. Ruml, "Improved MDS-based localization," in *Proc. IEEE INFOCOM*, 2003, pp. 2640–2651.

[13] J. S. Esteves, A. Carvalho, and C. Couto, "Generalized geometric triangulation algorithm for mobile robot absolute self-localization," in *Proc. IEEE Int. Symp. Ind. Electron.*, 2003, pp. 1–6.

[14] A. Alessandri and M. Gaggero, "Fast moving horizon state estimation for discrete-time systems using single and multi iteration descent methods," *IEEE Trans. Autom. Control*, vol. 62, no. 9, pp. 4499–4511, Sep. 2017.

[15] A. Ledergerber, M. Hamer, and R. D'Andrea, "A robot self-localization system using one-way ultra-wideband communication," in *Proc. IEEE/RSJ Int. Conf. Intell. Robots Syst.*, 2015, pp. 3131–3137.

[16] M. W. Mueller, M. Hamer, and R. D'Andrea, "Fusing ultra-wideband range measurements with accelerometers and rate gyroscopes for quadrocopter state estimation," in *Proc. IEEE Int. Conf. Robot. Autom.*, Seattle, WA, USA, 2015, pp. 1730–1736.

[17] K. Guo *et al.*, "Ultra-wideband based localization for quadcopter navigation," *Unmanned Syst.*, vol. 4, no. 1, pp. 23–34, 2016.

[18] Z. Chen, Q. Zhu, and Y. C. Soh, "Smartphone inertial sensor-based indoor localization and tracking with iBeacon corrections," *IEEE Trans. Ind. Informat.*, vol. 12, no. 4, pp. 1540–1549, Aug. 2016.

[19] T. Van Nguyen, Y. Jeong, H. Shin, and M. Z. Win, "Machine learning for wideband localization," *IEEE J. Sel. Areas Commun.*, vol. 33, no. 7, pp. 1357–1380, Jul. 2015.

[20] M. A. Alsheikh, S. Lin, D. Niyato, and H.-P. Tan, "Machine learning in wireless sensor networks: Algorithms, strategies, and applications," *IEEE Commun. Surveys Tuts.*, vol. 16, no. 4, pp. 652–656, 4th Quart., 2015.

[21] C. Wang, J. Yang, L. Xie, and J. Yuan, "Kervolutional neural networks," in *Proc. IEEE Conf. Comput. Vis. Pattern Recognit.*, 2019, pp. 31–40.

[22] T. M. Nguyen, A. H. Zaini, K. Guo, and L. Xie, "An ultra-wideband based multi-UAV localization system in GPS-denied environments," in *Proc. Int. Micro Air Veh. Conf. Competition*, 2016, pp. 1–6.
[23] W. Cui *et al.*, "Received signal strength based indoor positioning using a random vector functional link network," *IEEE Trans. Ind. Informat.*, vol. 14, no. 5, pp. 1846–1855, May 2018.
[24] R. Kümmerle, G. Grisetti, H. Strasdat, K. Konolige, and W. Burgard, "G^2o: A general framework for graph optimization," in *Proc. IEEE Int. Conf. Robot. Autom.*, 2011, pp. 3607–3613.
[25] Z. Lin, M. Fu, and Y. Diao, "Distributed self localization for relative position sensing networks in 2D space," *IEEE Trans. Signal Process.*, vol. 63, no. 14, pp. 3751–3761, Jul. 2015.
[26] C. Di Franco *et al.*, "Calibration-free network localization using non-line-of-sight ultra-wideband measurements," in *Proc. 16th ACM/IEEE Int. Conf.*, 2017, pp. 235–246.
[27] X. Li, X. Luo, and S. Zhao, "Globally convergent distributed network localization using locally measured bearings," *IEEE Trans. Control Netw. Syst.*, to be published.
[28] C. Wang, H. Zhang, T.-M. Nguyen, and L. Xie, "Ultra-wideband aided fast localization and mapping system," in *Proc. IEEE/RSJ Int. Conf. Intell. Robots Syst.*, 2017, pp. 1602–1609.
[29] X. Fang, C. Wang, T.-M. Nguyen, and L. Xie, "Model-free approach for sensor network localization with noisy distance measurement," in *Proc. 15th Int. Conf. Control Autom. Robot. Vis. (ICARCV)*, 2018, pp. 1973–1978.
[30] H. C. Brian, *Lie Groups, Lie Algebras, and Representations*. Cham, Switzerland: Springer Int., 2015.
[31] A. Benini, A. Mancini, and S. Longhi, "An IMU/UWB/vision-based extended Kalman filter for mini-UAV localization in indoor environment using 802.15.4a wireless sensor network," *J. Intell. Robot. Syst.*, vol. 70, pp. 461–476, Aug. 2012.
[32] G. Pillonetto, A. Aravkin, and S. Carpin, "The unconstrained and inequality constrained moving horizon approach to robot localization," in *Proc. IEEE/RSJ Int. Conf. Intell. Robots Syst.*, 2010, pp. 3830–3835.
[33] K. Kimura, Y. Hiromachi, K. Nonaka, and K. Sekiguchi, "Vehicle localization by sensor fusion of LRS measurement and odometry information based on moving horizon estimation," in *Proc. IEEE Conf. Control Appl.*, 2014, pp. 1306–1311.
[34] A. Simonetto, D. Balzaretti, and T. Keviczky, "A distributed moving horizon estimator for mobile robot localization problems," in *Proc. World Congr.*, vol. 18, no. 1, 2011, pp. 8902–8907.
[35] S. Wang, L. Chen, D. Gu, and H. Hu, "An optimization based moving horizon estimation with application to localization of autonomous underwater vehicles," *Robot. Auton. Syst.*, vol. 62, no. 10, pp. 1581–1596, 2014.
[36] F. Girrbach, J. D. Hol, G. Bellusci, and M. Diehl, "Optimization-based sensor fusion of GNSS and IMU using a moving horizon approach," *Sensors*, vol. 17, no. 5, pp. 1159–1165, 2017.
[37] C. Forster, L. Carlone, F. Dellaert, and D. Scaramuzza, *IMU Preintegration on Manifold for Efficient Visual-Inertial Maximum-a-Posteriori Estimation*, Georgia Inst. Technol., Atlanta, GA, USA, 2015.
[38] X. Longluo, L. Zhiliao, and H. WahTam, "Convergence analysis of the Levenberg–Marquardt method," *Optim. Methods Softw.*, vol. 22, no. 4, pp. 659–678, 2007.
[39] M. Williams and T. Munzner, "Steerable, progressive multidimensional scaling," in *Proc. IEEE Symp. Inf. Visual.*, 2004, pp. 57–64.
[40] Y. Chen, T. A. Davis, W. W. Hager, and S. Rajamanickam, "Algorithm 887: Cholmod, supernodal sparse cholesky factorization and update/downdate," *ACM Trans. Math. Softw.*, vol. 35, no. 3, pp. 22–30, 2008.
[41] A. Prorok and A. Martinoli, "Accurate indoor localization with ultra-wideband using spatial models and collaboration," *Int. J. Robot. Res.*, vol. 33, no. 4, pp. 547–568, 2014.
[42] Z. Chen and J. Wang, "GROF: Indoor localization using a multiple-bandwidth general regression neural network and outlier filter," *Sensors*, vol. 18, no. 11, pp. 3723–3730, 2018.

Xu Fang received the B.Eng. degree in electrical engineering from Beijing Forestry University, Beijing, China, in 2013, and the M.Sc. degree in control theory and control engineering from BeiHang University, Beijing, in 2016. He is currently pursuing the Ph.D. degree with the School of Electrical and Electronic Engineering, Nanyang Technological University, Singapore.

His research interests include cooperative control, unmanned systems, indoor localization and robot navigation.

Chen Wang received the B.Eng. degree from the Beijing Institute of Technology, Beijing, China, in 2014, and the Ph.D. degree in electrical engineering from Nanyang Technological University, Singapore, in 2019.

He is currently a Postdoctoral Fellow with Robotics Institute, Carnegie Mellon University, Pittsburgh, PA, USA. His research interests include robot perception, vision, and machine learning.

Thien-Minh Nguyen was born in Can Tho, Vietnam, in 1991. He received the B.Eng. degree in control engineering and automation from the Ho Chi Minh City University of Technology (member of Vietnam National University), Ho Chi Minh City, Vietnam, in 2014. He is currently pursuing the Ph.D. degree with the School of Electrical and Electronic Engineering, Nanyang Technological University, Singapore.

His research interests include multirobot localization and control, localization in GPS-denied environments, and UAV systems.

Lihua Xie (Fellow, IEEE) received the B.E. and M.E. degrees in electrical engineering from the Nanjing University of Science and Technology, Nanjing, China, in 1983 and 1986, respectively, and the Ph.D. degree in electrical engineering from the University of Newcastle, Callaghan, NSW, Australia, in 1992.

Since 1992, he has been with the School of Electrical and Electronic Engineering, Nanyang Technological University, Singapore, where he is currently a Professor and the Director of Delta-NTU Corporate Laboratory for Cyber-Physical Systems. He served as the Head of Division of Control and Instrumentation from July 2011 to June 2014. He held teaching appointments with the Department of Automatic Control, Nanjing University of Science and Technology, Nanjing, China, from 1986 to 1989. His research interests include robust control and estimation, networked control systems, multiagent networks, and localization and unmanned systems.

Prof. Xie is an Editor-in-Chief of *Unmanned Systems* and an Associate Editor of the IEEE TRANSACTIONS ON CONTROL OF NETWORK SYSTEMS. He has served as an Editor for *IET Book Series in Control* and an Associate Editor for a number of journals, including the IEEE TRANSACTIONS ON AUTOMATIC CONTROL, *Automatica*, IEEE TRANSACTIONS ON CONTROL SYSTEMS TECHNOLOGY, and IEEE TRANSACTIONS ON CIRCUITS AND SYSTEMS—PART II: ANALOG AND DIGITAL SIGNAL PROCESSING. He was an Elected Member of Board of Governors of IEEE Control System Society January 2016 to December 2018. He is a fellow of IFAC in 2007.